

Non-Hermitian Exceptional Landau Quantization in Electric Circuits

Xiao-Xiao Zhang  and Marcel Franz

Department of Physics and Astronomy & Stewart Blusson Quantum Matter Institute, University of British Columbia, Vancouver, British Columbia, V6T 1Z4 Canada

 (Received 22 September 2019; published 30 January 2020)

Alternating current *RLC* electric circuits form an accessible and highly tunable platform simulating Hermitian as well as non-Hermitian (NH) quantum systems. We propose here a circuit realization of NH Dirac and Weyl Hamiltonians subject to time-reversal invariant pseudomagnetic field, enabling the exploration of novel NH physics. We identify the low-energy physics with a generic real energy spectrum from the NH Landau quantization of exceptional points and rings, which can avoid the NH skin effect and provides a physical example of a quasiparticle moving in the complex plane. Realistic detection schemes are designed to probe the flat energy bands, sublattice polarization, edge states protected by a NH energy-reflection symmetry, and a characteristic nodeless probability distribution.

DOI: 10.1103/PhysRevLett.124.046401

Introduction.—Hermiticity of Hamiltonians has long been a required ingredient in any self-consistent framework of quantum theory for both the stationary and time-dependent problems. There has been an increasing effort aimed at understanding the phenomena resultant from relaxing the Hermiticity condition both as a theoretical challenge and as a description of various physical systems [1]. Theoretical and experimental efforts were largely ignited by the recognition of the parity-time (*PT*) symmetry [2,3], its realization in optics [4–6], and further generalizations [7,8]. In physical systems non-Hermiticity can arise through incorporating loss or gain but also by viewing Hermitian systems from new angles, including vortex pinning in superconductors [9], topological surface state [10,11], and quasiparticles with self-energy correction [12–15]. Important developments have recently been focused on the classification of new phases [16–27], the bulk Fermi arc and line structures [12,15,28,29] and the anomalous bulk-boundary correspondence with the skin effect where macroscopically many states are localized at the boundary [30–41]. Of particular importance are the generic exceptional degeneracies—exceptional point (EP) in two dimensions (2D) and exceptional ring (ER) in three dimensions (3D)—in the complex energy spectrum where two resonances match at once in position and width [42–47]. Signatures have been experimentally observed in microwave cavities [48,49], exciton-polariton systems [50], and photonic lattices [51,52].

In this Letter we discuss a new family of phenomena arising from applying magnetic field to nontrivial non-Hermitian (NH) systems. This problem has remained largely unexplored owing to the lack of a feasible realization which we overcome here by considering a convenient synthetic platform based on alternating current (ac) circuits. Periodic arrays of capacitors and inductors are known to

simulate the physics of electrons in crystal lattices and can model various topological phases [53–65]. We introduce NH effects by including dissipative resistance in such arrays. Pseudomagnetic fields (PMFs) can be generated by spatially varying certain electric elements, which extends to the NH case the PMF realized by elastic strain in relativistic electron systems [66–72]. The NH effects generically turn relativistic band crossings into exceptional degeneracies. Interplay with the PMF then results in a novel NH low-energy theory of *bulk* states which have a *real* energy spectrum and are free from the skin aggregation effect. In addition such systems exhibit novel edge states protected by strong NH energy-reflection symmetry and realize a physical analog of a particle moving in the complex domain. We explain how these remarkable phenomena can be detected via conventional electric measurements.

Circuit realization.—Based on the Kirchhoff current law (KCL), one can apply the node analysis to an ac circuit at frequency ω . The Euler-Lagrange equation for the node flux variable φ_j given the external current i_j injected at node j reads

$$\frac{d}{dt} \frac{\partial L}{\partial \dot{\varphi}_j} - \frac{\partial L}{\partial \varphi_j} + \frac{\partial D}{\partial \dot{\varphi}_j} = i_j, \quad (1)$$

where for capacitors and inductors $L_C = \frac{C}{2} \dot{\varphi}^2$, $L_L = -\frac{1}{2L} \varphi^2$ while Rayleigh dissipation function $D = \frac{1}{2R} \dot{\varphi}^2$ describes resistors. These equations form an admittance problem, $J\mathbf{v} = \mathbf{i}$, where the admittance matrix J determines the voltage response $\mathbf{v} = \dot{\boldsymbol{\varphi}}$ in the circuit to an array of injected currents $\mathbf{i} = (i_1, i_2, \dots, i_N)$. At any fixed frequency J can be mapped to a tight-binding Hamiltonian $H = -iJ$ with hopping amplitudes ωC ($\frac{1}{\omega L}$) for nodes connected by a capacitor (inductor) while a NH hopping i/R accounts for

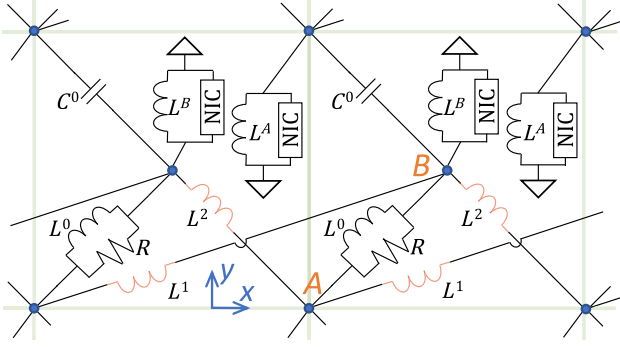


FIG. 1. RLC circuit simulating a quantum system with Dirac dispersions which turn into exceptional degeneracies upon inclusion of NH effects. PMF defined by gauge potential $A_y = bx$ can be generated by varying the red elements along the x direction. Linear variation, required for uniform PMF, dictates open boundary condition along x .

any resistor and hence $H(R \mapsto -R) = H^\dagger$. Lossless LC circuits can fully simulate ordinary time-reversal (\mathcal{T}) invariant quantum Hamiltonians as the π -phase difference between L, C hoppings suggests. This remains true in the presence of PMF which couples to Dirac or Weyl nodes in a way that respects \mathcal{T} . Solving the eigenproblem $H|\psi_\alpha\rangle = E_\alpha|\psi_\alpha\rangle$ corresponds to finding a spatial pattern of currents \mathbf{i}_α that produces the identical pattern of voltages $iE_\alpha v_\alpha = \mathbf{i}_\alpha$. We discuss later how circuit tomography connects standard impedance or voltage measurements with the energy spectrum and the wave function of the quantum problem.

Here we focus on periodic circuits described by a family of two-band Bloch Hamiltonians $h(\mathbf{k}) = d_0\mathbb{1} + \sum_i d_i\sigma_i$ where pseudospin σ stands for inequivalent nodes A, B . As described in Supplemental Material [73], following the mapping between quantum model and ac KCL, a square-lattice circuit depicted in Fig. 1 can realize a variety of Hamiltonians of this type. Specifically, the circuit in Fig. 1 is described by

$$\begin{aligned} d_x &= i\gamma - \kappa_1 + \kappa \cos k_y - t_x \cos k_x, \\ d_y &= t_y \sin k_y - \kappa_2 \sin k_x, \end{aligned} \quad (2)$$

with a staggered on site potential $d_z = \Delta$. The relation to circuit element parameters is $\gamma = \frac{1}{R}$, $\kappa_1 = \frac{1}{\omega L^0}$, $\kappa = t_y = \omega C^0$, $t_x = \frac{1}{\omega}(\frac{1}{L^1} + \frac{1}{L^2})$, $\kappa_2 = \frac{1}{\omega}(\frac{1}{L^2} - \frac{1}{L^1})$, and $\Delta = \frac{1}{2\omega}(\frac{1}{L^A} - \frac{1}{L^B})$. Gain from the negative impedance converter (NIC) compensates for the loss incurred in the resistor R enabling unimpeded signal propagation through the array [74–77]. Dissipation for NH effect and spatially nonuniform elements for PMF can make d_0 , respectively, complex and inhomogeneous as per the mapping. As explained in the Supplemental Material, the NIC element acting as a static negative resistor, together with other tunable grounded elements, guarantees a real-valued and uniform d_0 in analogy to a controllable chemical potential.

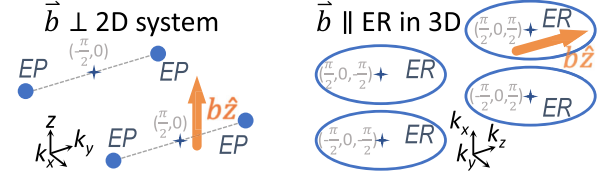


FIG. 2. Exceptional degeneracies in 2D and 3D circuit models generated by NH terms. Dashed bulk Fermi arc connects two EPs. Real energy spectrum emerges when PMF \mathbf{b} takes the direction noted. In circuit calculations, we fix $\mathbf{b} = b\hat{z}$ for one exceptional degeneracy region as indicated.

The circuit in Fig. 1 realizes relativistic band structures similar to graphene in a simpler square lattice. When $\gamma = \Delta = \kappa_2 = 0$ and $\kappa = \kappa_1$, the Hermitian spectrum $E_{\mathbf{k}}$ of $h(\mathbf{k})$ without PMF, exhibits a pair of Dirac points located at $(\pm\frac{\pi}{2}, 0)$ with Fermi velocity $v_F^i = t_i$ in the i direction. As illustrated in Fig. 2 inclusion of the dissipative term $i\gamma\sigma_x$ with $\gamma > \Delta$ splits each Dirac point into a pair of EPs at $(\pm\frac{\pi}{2}, \pm\sqrt{\gamma^2 - \Delta^2}/v_F^y)$ at low energy. Each EP pair is connected by a bulk Fermi arc, indicated by dashed lines in Fig. 2, along which the real part $\Re E_{\mathbf{k}}$ of the two bands touches [12,15] (see also Sec. III in the Supplemental Material [73]). We also consider a 3D cubic lattice non-centrosymmetric model of four parallel Weyl ERs depicted in Fig. 2 and constructed by layering the 2D EP circuit along the z axis with interlayer connections determined by $d_z = -t_z \cos k_z$ [73].

A special feature of relativistic dispersions lies in that spatially varying hopping amplitudes can act as vector potentials chirally coupled to the low-energy excitations [66–69]. This feature naturally extends to the exceptional degeneracies when NH terms are included. A linear variation along the x direction in inductances of the red elements in Fig. 1 produces spatial variation of the Hamiltonian parameter $\kappa_2 = v_F^y bx$ and dictates open boundary along x . In the low-energy theory this manifests as a Landau gauge $A_y = bx$ giving rise to a uniform PMF $b\hat{z}$. Vector potential $A_x = -by$ can also be realized by varying $\kappa_1 = \kappa - v_F^x by$ along the y direction with open edges, see Fig. S1 in the Supplemental Material [73].

NH exceptional Landau levels.—Band structure of the EP circuit is displayed in Fig. 3, where exceptional degeneracies are eliminated by the PMF illustrated in Fig. 2. Surprisingly, the resulting Landau-level-like flat bands exhibit spectra with consistently *vanishing* imaginary part around the exceptional degeneracies. To understand this remarkable feature we first develop a low-energy theory of this NH Landau quantization of exceptional degeneracy and then discuss the origin of purely real spectrum.

The low-energy Hamiltonian around the exceptional region with the magnetic field $b\hat{z}$ indicated in Fig. 2 reads

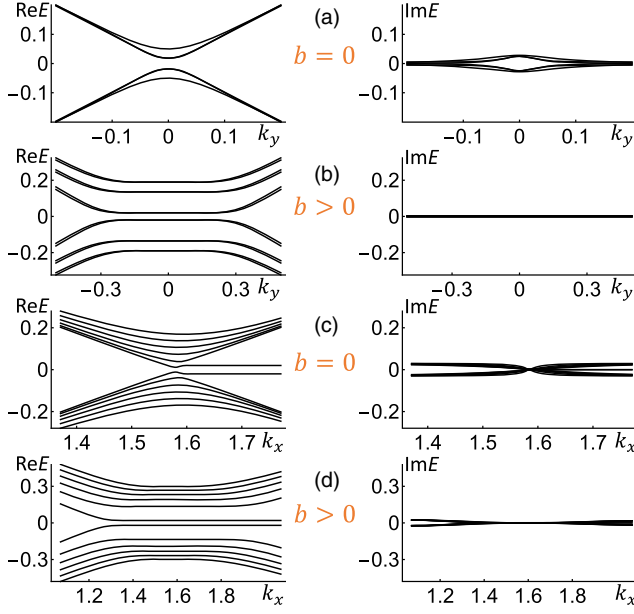


FIG. 3. Band structure of the 100×100 square lattice EP circuit. Panels (a), (b) have open boundaries along x realizing armchair-like bands under gauge $A_y = bx$ while panels (c), (d) have open boundaries along y realizing zigzag-like bands under gauge $A_x = -by$. 3D Weyl ER case at $k_z = \frac{\pi}{2} + \Delta/t_z$ is the same as (c), (d). (See the Supplemental Material [73] for extended discussion of the $b = 0$ case.) We set $t_i = 1$, unmodulated $\kappa = \kappa_1 = 1$, $\kappa_2 = 0$, and $\Delta = 0.02$, $\gamma = 0.03$, $b = 0.009$.

$$h = \sum_{i=x,y} (v_F^i \Pi_i + i\gamma_i) \sigma_i + \Delta \sigma_z = \begin{bmatrix} \Delta & E_b f_+ \\ E_b f_- & -\Delta \end{bmatrix}, \quad (3)$$

where $v_F^i, b > 0$, $E_b = \sqrt{2v_F^x v_F^y b}$ and $\Pi_i = p_i - A_i$. Momentum operator $p_i = -i\partial_i$ may be replaced by k_i along the periodic direction of the circuit. Δ is replaced by $v_F^z k_z$ for the 3D ER case. Furthermore

$$f_{\mp} = (v_F^x \Pi_x \pm i v_F^y \Pi_y + i\gamma_x \mp \gamma_y) / E_b. \quad (4)$$

The first observation is that $[f_-, f_+] = 1$ formally holds, even though $f_{\pm}^{\dagger} \neq f_{\pm}$. Second, if $f_- \phi_0 = 0$ has a physical square-integrable solution, one can construct a tower of NH Landau levels (LL) through the wave function ansatz $\psi_n = (\alpha \phi_n, \beta \phi_{n-1})^T$ for $n = 0, 1, 2, \dots$ where $\phi_{-1} = 0$ and $\phi_{n>0}$ is obtained by the relation $f_+ \phi_n = \sqrt{n+1} \phi_{n+1}$, $f_- \phi_n = \sqrt{n} \phi_{n-1}$. An explicit calculation then gives energy of the n th NH LL (LL_n) $E_{LL_{n\pm}} = \pm \sqrt{\Delta^2 + nE_b^2}$ when $n \geq 1$ and $E_{LL_{0+}} = \Delta$ when $n = 0$, which is isospectral to the Hermitian counterpart. The construction is valid for arbitrary γ_x, γ_y but breaks down in the presence of nonzero $i\gamma_z \sigma_z$. As this tilts the ER plane, requiring PMF||ER is thus the major difference in the 3D case in Fig. 2.

For the above procedure to work it is essential to ensure a physical solution of $f_- \phi_0 = 0$, the existence of which is not

guaranteed in the NH case. Imagine for instance a spatially linear modulation of the resistors in the circuit, which can introduce an *imaginary*-valued vector potential, e.g., $A_x = -iby$ and hence $[f_-, f_+] = i$ with a tower of complex LLs. In this case, however, a normalizable bounded solution of $f_- \phi_0 = 0$ does not exist [80]. We proceed as an example with our real-valued $A_x = -by$ that has a valid normalized wave function

$$\phi_n = (\sqrt{\pi} l_b n! 2^n)^{-\frac{1}{2}} e^{-(y-y_0)^2/2l_b^2 + \gamma_y y} H_n[(y-y_0)/l_b] \quad (5)$$

where $y_0 = -(k_x + i\gamma_x)/b$, magnetic length $l_b = b^{-1/2}$ and $H_n(\mathbf{z})$ is the Hermite polynomial valued in the complex \mathbf{z} plane. Note that γ_x renders ϕ_n complex valued while γ_y breaks its symmetry with respect to the Hermitian oscillation center $y = -k_x/b$. Henceforth we mainly consider the case with $\gamma_y = 0$ which emerges naturally from our circuit realization. In general, NH systems have the potential for skin effect, which deviates from the Bloch band theory and the conventional bulk-boundary correspondence [30–34,36]. Remarkably here, not only is any possible skin aggregation suppressed in the low-energy regime as dictated by the *bulk* magnetic confinement around y_0 at the length scale $\sqrt{n+1}/2l_b$, but also the NH quasiparticle is now oscillating along a *complex* y -direction line centered at y_0 . Therefore, this NH system under magnetic field indicates a new way to avoid the skin effect and provides a concrete example of a quasiparticle moving in the complex domain. This latter scenario is justified by the Hermite function actually being holomorphic on \mathbb{C} , although it is usually viewed solely as a real function in conventional quantum problems. The orthonormality, $\int_{-\infty}^{\infty} dy \phi_n(\mathbf{z}) \phi_m(\mathbf{z}) = \delta_{mn}$ with $\mathbf{z} = (y-y_0)/l_b$, follows from analytic continuation. This way, one can also interpret the problem as analytically continuing the particle motion to the complex domain.

Spectral properties.—Our NH low-energy theory has a real spectrum under finite PMF although it is not \mathcal{PT} symmetric. To understand this one can formalize the above physical interpretation of a quasiparticle moving in the complex plane by defining an operator $\rho = \text{diag}(e^{\epsilon p}, e^{\epsilon^* p})$ that translates the system in real space along the imaginary direction by $\epsilon = \frac{1}{b} \hat{z} \times \boldsymbol{\gamma}$ for $\boldsymbol{\gamma} = \gamma_x \hat{x}$. The pseudo-Hermiticity [7,8], a necessary but *not sufficient* condition for a real spectrum, $\eta h \eta^{-1} = h^{\dagger}$, holds here via a positive semidefinite Hermitian automorphism $\eta = \rho^{\dagger} \rho$. In addition one can deduce the spectral reality via a similarity transformation $\rho h \rho^{-1} = h_0 = h(\boldsymbol{\gamma} = 0)$ which in general preserves the spectrum and maps h to a Hermitian Hamiltonian with a spectral expansion $h_0 = \sum_n E_n |\varphi_n\rangle \langle \varphi_n|$ of real-spectrum conventional LLs. Then the left and right eigenstates, corresponding to Eq. (5), respectively, of h^{\dagger} and h are given by $|\psi_n^{L(R)}\rangle = \rho^{-1(\dagger)} |\varphi_n\rangle$. Hence the biorthogonal representation [1,81], $h = \sum_n E_n |\psi_n^L\rangle \langle \psi_n^R|$, naturally follows. The aforementioned orthonormality based on

NH Hermite functions helps prove herein the general pseudo-Hermitian orthonormality and biorthonormality $\langle \psi_m^L | \eta | \psi_n^L \rangle = \langle \psi_m^R | \psi_n^L \rangle = \delta_{mn}$.

Physically, the magnetic field in a relativistic system is crucial to the above reasoning. The phenomenon can be viewed as cancelling γ by absorbing it into the vector potential A in the kinetic term. This relies on A depending linearly on the spatial coordinate, necessary to give a uniform b field. One may wonder about the dual picture of translating by γ in the imaginary direction of the momentum space by using $e^{\gamma \cdot x}$ in ρ with position operator x , which actually explains under the gauge used the $e^{\gamma \cdot y}$ factor in Eq. (5) by setting $\gamma = \gamma_y \hat{y}$. It also relies on a finite b , otherwise the wave function $|\psi_n^{L(R)}\rangle$ is unbounded. Therefore, magnetic field imparts a nonperturbative change to the system. The phenomenon and interpretation applies as well to the symmetric gauge, which we employ to construct the NH ground state and coherent state in the Supplemental Material [73].

Detection schemes.—Based on the KCL construction, one can readily predict the directly measurable electrical response of the circuit. We consider two types of circuit tomography assuming system size $L_x \times L_y$, (i) impedance scan $Z_{(x,0),(x,y)}^{s_0 s}$ (d_0) reflecting a direct impedance measurement between two points $(x, 0, s_0)$ and (x, y, s) , and (ii) voltage scan $V_{(x_0, y_0),(x,y)}^{s_0 s}$ (d_0) probing voltage at any node (x, y, s) in response to a current input at the midpoint $y_0 = L_y/2$ of the $x_0 = 0, L_x/2$ lines, where $s, s_0 = A, B$. We derive in the Supplemental Material [73] expressions for both quantities in terms of left and right eigenstates of the NH Hamiltonian.

Several observations can be made based on the predictions for impedance and voltage scans in Fig. 4. First, in order to have a significant voltage response, large density of states within a small range of admittance eigenvalue j is required. Compared to topological boundary zero modes [56], this is naturally achieved in the presence of PMF by the flat NH LLs, which can be set in resonance by controlling d_0 . An example of this enhancement is given in Figs. 4(a)–4(d). Second, a unique sublattice polarization of the lowest LL (LL_0) and the general wave function form $\psi_n = (\alpha \phi_n, \beta \phi_{n-1})^T$ hold for the exceptional LLs. Controlling d_0, s_0, s , sublattice-resolved responses provide access to this. The armchair-like case has every NH LL doubly degenerate in a PMF while the zigzag-like case mixes the NH LL_0 s with the edge states. Below we use both to highlight different features.

Edge state from NH energy-reflection symmetry.—Consider the EP circuit in resonance at $d_0 = E_{LL_{0\pm}} = \pm \Delta$, i.e., the positive or negative $LL_{0\pm}$ in Fig. 3(b). One thus has dichotomous choices in d_0, s_0, s and $x_0 = 0, L_x/2$. Figures 4(a), 4(c) and 4(b), 4(d) illustrate the *only* two enhanced cases respectively of bulk and edge nature as seen from the pronounced signal distribution contrast. All others are largely suppressed or vanishing. The edge state

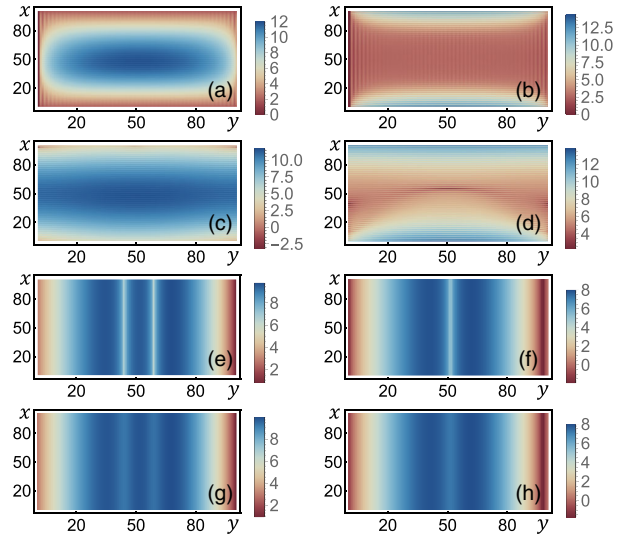


FIG. 4. Impedance and voltage tomography for the NH circuit used in Fig. 3. Amplitudes are plotted on logarithmic scale for armchair-like (a), (b), (c), (d) and zigzag-like (e), (f), (g), (h) cases. Panels (a), (b), (c), (d) show two cases with strongly enhanced response for $LL_{0\pm}$ in resonance. Impedance scan (a) $Z_{(x,0),(x,y)}^{AA}(E_{LL_{0+}})$, (b) $Z_{(x,0),(x,y)}^{BB}(E_{LL_{0-}})$ and voltage scan (c) $V_{(L_x/2, L_y/2),(x,y)}^{AA}(E_{LL_{0+}})$, (d) $V_{(0, L_y/2),(x,y)}^{BB}(E_{LL_{0-}})$. Panels (e), (f), (g), (h) show voltage scan displaying NH nodeful-nodeless transition of the up (ϕ_2) and down (ϕ_1) wave function component of the LL_{2+} in resonance. (e) Hermitian, (g) NH $V_{(x,y)}^{AA}(E_{LL_{2+}})$ and (f) Hermitian, (h) NH $V_{(x,y)}^{BB}(E_{LL_{2+}})$.

LL_{0-} localized around $x_0 = 0, L_x$, surprisingly, cannot be captured in a low-energy NH two-flavour 2D massive Dirac theory under PMF, which solely leads to two degenerate LL_{0+} states. Analyzed in the Supplemental Material [73], it is actually the consequence of a strong lattice NH energy-reflection symmetry for *any* Hermitian or NH bipartite hoppings which is beyond the usually pertinent chiral or particle-hole symmetry. These confirm the NH sublattice polarization from an intricate interplay between the PMF, Dirac mass, armchair-like bands, and the NH symmetry that dictates pairs of opposite and however complex or real bands.

NH nodeless wave function.—Observation of the non-Hermiticity is most prominent via inspecting the wave functions because of the spectral property discussed. The two-component general wave function form here becomes relevant. One can combine the nodal structure of conventional Hermite functions, i.e., $H_n(y)$ possesses n nodes, with our physical interpretation of translating the motion to the complex plane of $H_n(z)$. This directly leads to the removal of all nodes by the finite $\Im z = \epsilon$. Therefore, a transition from nodeful to *nodeless* probability (voltage) distribution becomes a distinguishing NH feature. This is made practically feasible by the quantum superposition principle; i.e., one can inject spatially sinusoidally

oscillating current at a certain wave number k'_x along one single open boundary, say, the $y = 0$ edge of the EP circuit, which suffices to extract the NH Hermite wave function associated with k'_x . Figures 4(e), 4(g) and 4(f), 4(h) exemplify this nodeful-nodeless transition of ϕ_2 and ϕ_1 , respectively, by plotting the amplitude of voltage response.

Outlook.—Using specially designed ac electric circuits we develop a theory and present detection schemes for a unique NH low-energy real spectrum without skin effect, which arise from the relativistic exceptional degeneracies under magnetic field and exhibit NH symmetry protected edge state and quasiparticle moving in the complex domain. These results enrich a novel platform for synthetic quantum systems and lay the groundwork for future investigations of the interplay between non-Hermiticity and the magnetic field, which is relevant to the emerging real quantum systems with exceptional degeneracies [48–52]. Various intriguing questions are to be explored ahead, including imaginary-valued vector potential or magnetic field, further generalization of quasiparticle living in the complex plane, NH quantum valley Hall effect in the EP circuit with PMF, and a possible NH Hofstadter butterfly readily realized by introducing resistors to the circuit of nodes with internal eigenmodes in a similar manner to the present study [54,58,73].

X.-X.Z appreciates discussions with R. Haenel, W. Yang, É. Lantagne-Hurtubise, and T. Liu. Research described in this Letter was supported by NSERC and by CIFAR.

-
- [1] N. Moiseyev, *Non-Hermitian Quantum Mechanics* (Cambridge University Press, Cambridge, England, 2009), <http://dx.doi.org/10.1017/cbo9780511976186>.
- [2] C. M. Bender and S. Boettcher, *Phys. Rev. Lett.* **80**, 5243 (1998).
- [3] C. M. Bender, *Rep. Prog. Phys.* **70**, 947 (2007).
- [4] K. G. Makris, R. El-Ganainy, D. N. Christodoulides, and Z. H. Musslimani, *Phys. Rev. Lett.* **100**, 103904 (2008).
- [5] A. Guo, G. J. Salamo, D. Duchesne, R. Morandotti, M. Volatier-Ravat, V. Aimez, G. A. Siviloglou, and D. N. Christodoulides, *Phys. Rev. Lett.* **103**, 093902 (2009).
- [6] C. E. Rüter, K. G. Makris, R. El-Ganainy, D. N. Christodoulides, M. Segev, and D. Kip, *Nat. Phys.* **6**, 192 (2010).
- [7] A. Mostafazadeh, *J. Phys. A* **36**, 7081 (2003).
- [8] A. Mostafazadeh, *Int. J. Geom. Methods Mod. Phys.* **07**, 1191 (2010).
- [9] N. Hatano and D. R. Nelson, *Phys. Rev. Lett.* **77**, 570 (1996).
- [10] J. González and R. A. Molina, *Phys. Rev. B* **96**, 045437 (2017).
- [11] R. A. Molina and J. González, *Phys. Rev. Lett.* **120**, 146601 (2018).
- [12] V. Kozii and L. Fu, [arXiv:1708.05841](https://arxiv.org/abs/1708.05841).
- [13] H. Shen and L. Fu, *Phys. Rev. Lett.* **121**, 026403 (2018).
- [14] A. A. Zyuzin and A. Y. Zyuzin, *Phys. Rev. B* **97**, 041203 (2018).
- [15] M. Papaj, H. Isobe, and L. Fu, *Phys. Rev. B* **99**, 201107 (2019).
- [16] D. Leykam, K. Y. Bliokh, C. Huang, Y. D. Chong, and F. Nori, *Phys. Rev. Lett.* **118**, 040401 (2017).
- [17] Y. Ashida, S. Furukawa, and M. Ueda, *Nat. Commun.* **8**, 15791 (2017).
- [18] H. Shen, B. Zhen, and L. Fu, *Phys. Rev. Lett.* **120**, 146402 (2018).
- [19] K. Kawabata, S. Higashikawa, Z. Gong, Y. Ashida, and M. Ueda, *Nat. Commun.* **10**, 297 (2019).
- [20] Z. Gong, Y. Ashida, K. Kawabata, K. Takasan, S. Higashikawa, and M. Ueda, *Phys. Rev. X* **8**, 031079 (2018).
- [21] V. M. M. Alvarez, J. E. B. Vargas, M. Berdakin, and L. E. F. F. Torres, *Eur. Phys. J. Spec. Top.* **227**, 1295 (2018).
- [22] S. Lin, L. Jin, and Z. Song, *Phys. Rev. B* **99**, 165148 (2019).
- [23] K. L. Zhang, H. C. Wu, L. Jin, and Z. Song, *Phys. Rev. B* **100**, 045141 (2019).
- [24] Z. Yang and J. Hu, *Phys. Rev. B* **99**, 081102 (2019).
- [25] H. Wang, J. Ruan, and H. Zhang, *Phys. Rev. B* **99**, 075130 (2019).
- [26] A. Ghatak and T. Das, *J. Phys. Condens. Matter* **31**, 263001 (2019).
- [27] L. E. F. F. Torres, *J. Phys. Mater.* **3**, 014002 (2019).
- [28] H. Zhou, C. Peng, Y. Yoon, C. W. Hsu, K. A. Nelson, L. Fu, J. D. Joannopoulos, M. Soljačić, and B. Zhen, *Science* **359**, 1009 (2018).
- [29] J. Carlström and E. J. Bergholtz, *Phys. Rev. A* **98**, 042114 (2018).
- [30] T. E. Lee, *Phys. Rev. Lett.* **116**, 133903 (2016).
- [31] V. M. M. Alvarez, J. E. B. Vargas, and L. E. F. F. Torres, *Phys. Rev. B* **97**, 121401 (2018).
- [32] Y. Xiong, *J. Phys. Commun.* **2**, 035043 (2018).
- [33] F. K. Kunst, E. Edvardsson, J. C. Budich, and E. J. Bergholtz, *Phys. Rev. Lett.* **121**, 026808 (2018).
- [34] S. Yao and Z. Wang, *Phys. Rev. Lett.* **121**, 086803 (2018).
- [35] S. Yao, F. Song, and Z. Wang, *Phys. Rev. Lett.* **121**, 136802 (2018).
- [36] K. Yokomizo and S. Murakami, *Phys. Rev. Lett.* **123**, 066404 (2019).
- [37] L. Jin and Z. Song, *Phys. Rev. B* **99**, 081103 (2019).
- [38] C. H. Lee and R. Thomale, *Phys. Rev. B* **99**, 201103 (2019).
- [39] M. Ezawa, *Phys. Rev. B* **99**, 121411 (2019).
- [40] T. Helbig, T. Hofmann, S. Imhof, M. Abdelghany, T. Kiessling, L. W. Molenkamp, C. H. Lee, A. Szameit, M. Greiter, and R. Thomale, [arXiv:1907.11562](https://arxiv.org/abs/1907.11562).
- [41] L. Xiao, T. Deng, K. Wang, G. Zhu, Z. Wang, W. Yi, and P. Xue, [arXiv:1907.12566](https://arxiv.org/abs/1907.12566).
- [42] M. Berry, *Czech. J. Phys.* **54**, 1039 (2004).
- [43] W. D. Heiss, *J. Phys. A* **45**, 444016 (2012).
- [44] Y. Xu, S.-T. Wang, and L.-M. Duan, *Phys. Rev. Lett.* **118**, 045701 (2017).
- [45] A. Cerjan, M. Xiao, L. Yuan, and S. Fan, *Phys. Rev. B* **97**, 075128 (2018).
- [46] R. Okugawa and T. Yokoyama, *Phys. Rev. B* **99**, 041202 (2019).
- [47] K. Luo, J. Feng, Y. X. Zhao, and R. Yu, [arXiv:1810.09231](https://arxiv.org/abs/1810.09231).

- [48] C. Dembowski, H.-D. Gräf, H. L. Harney, A. Heine, W. D. Heiss, H. Rehfeld, and A. Richter, *Phys. Rev. Lett.* **86**, 787 (2001).
- [49] C. Dembowski, B. Dietz, H.-D. Gräf, H. L. Harney, A. Heine, W. D. Heiss, and A. Richter, *Phys. Rev. E* **69**, 056216 (2004).
- [50] T. Gao, E. Estrecho, K. Y. Bliokh, T. C. H. Liew, M. D. Fraser, S. Brodbeck, M. Kamp, C. Schneider, S. Höfling, Y. Yamamoto, F. Nori, Y. S. Kivshar, A. G. Truscott, R. G. Dall, and E. A. Ostrovskaya, *Nature (London)* **526**, 554 (2015).
- [51] B. Zhen, C. W. Hsu, Y. Igarashi, L. Lu, I. Kaminer, A. Pick, S.-L. Chua, J. D. Joannopoulos, and M. Soljačić, *Nature (London)* **525**, 354 (2015).
- [52] A. Cerjan, S. Huang, M. Wang, K. P. Chen, Y. Chong, and M. C. Rechtsman, *Nat. Photonics* **13**, 623 (2019).
- [53] J. Ningyuan, C. Owens, A. Sommer, D. Schuster, and J. Simon, *Phys. Rev. X* **5**, 021031 (2015).
- [54] V. V. Albert, L. I. Glazman, and L. Jiang, *Phys. Rev. Lett.* **114**, 173902 (2015).
- [55] W. Zhu, S. Hou, Y. Long, H. Chen, and J. Ren, *Phys. Rev. B* **97**, 075310 (2018).
- [56] C. H. Lee, S. Imhof, C. Berger, F. Bayer, J. Brehm, L. W. Molenkamp, T. Kiessling, and R. Thomale, *Commun. Phys.* **1**, 39 (2018).
- [57] K. Luo, R. Yu, and H. Weng, *Research* **2018**, 6793752 (2018).
- [58] E. Zhao, *Ann. Phys. (Amsterdam)* **399**, 289 (2018).
- [59] M. Ezawa, *Phys. Rev. B* **98**, 201402 (2018).
- [60] S. Imhof, C. Berger, F. Bayer, J. Brehm, L. W. Molenkamp, T. Kiessling, F. Schindler, C. H. Lee, M. Greiter, T. Neupert, and R. Thomale, *Nat. Phys.* **14**, 925 (2018).
- [61] R. Haenel, T. Branch, and M. Franz, *Phys. Rev. B* **99**, 235110 (2019).
- [62] M. Ezawa, *Phys. Rev. B* **100**, 081401 (2019).
- [63] R. Yu, Y. X. Zhao, and A. P. Schnyder, *arXiv:1906.00883*.
- [64] Y. Lu, N. Jia, L. Su, C. Owens, G. Juzeliūnas, D. I. Schuster, and J. Simon, *Phys. Rev. B* **99**, 020302 (2019).
- [65] M. Serra-Garcia, R. Sūsstrunk, and S. D. Huber, *Phys. Rev. B* **99**, 020304 (2019).
- [66] F. Guinea, M. I. Katsnelson, and A. K. Geim, *Nat. Phys.* **6**, 30 (2010).
- [67] N. Levy, S. A. Burke, K. L. Meaker, M. Panlasigui, A. Zettl, F. Guinea, A. H. C. Neto, and M. F. Crommie, *Science* **329**, 544 (2010).
- [68] A. Cortijo, Y. Ferreirós, K. Landsteiner, and M. A. H. Vozmediano, *Phys. Rev. Lett.* **115**, 177202 (2015).
- [69] D. I. Pikulin, A. Chen, and M. Franz, *Phys. Rev. X* **6**, 041021 (2016).
- [70] V. Peri, M. Serra-Garcia, R. Ilan, and S. D. Huber, *Nat. Phys.* **15**, 357 (2019).
- [71] M. C. Rechtsman, J. M. Zeuner, A. Tünnermann, S. Nolte, M. Segev, and A. Szameit, *Nat. Photonics* **7**, 153 (2013).
- [72] P. Nigge, A. C. Qu, É. Lantagne-Hurtubise, E. Mårsell, S. Link, G. Tom, M. Zonno, M. Michiardi, M. Schneider, S. Zhdanovich, G. Levy, U. Starke, C. Gutiérrez, D. Bonn, S. A. Burke, M. Franz, and A. Damascelli, *Sci. Adv.* **5**, eaaw5593 (2019).
- [73] See the Supplemental Material at <http://link.aps.org/supplemental/10.1103/PhysRevLett.124.046401> for more details, which includes Refs. [54,58,74–79].
- [74] *Fundamentals of Circuits and Filters*, edited by W.-K. Chen, The Circuits and Filters Handbook 3rd ed. (CRC Press, Boca Raton, 2009), <https://doi.org/10.1201/9781315219134>.
- [75] T. H. Lee, *The Design of CMOS Radio-Frequency Integrated Circuits*, 2nd ed. (Cambridge University Press, Cambridge, England, 2003), <http://dx.doi.org/10.1017/cbo9780511817281>.
- [76] C. R. Popa, *Synthesis of Computational Structures for Analog Signal Processing* (Springer, New York, 2012), <http://dx.doi.org/10.1007/978-1-4614-0403-3>.
- [77] T. Hofmann, T. Helbig, C. H. Lee, M. Greiter, and R. Thomale, *Phys. Rev. Lett.* **122**, 247702 (2019).
- [78] É. Lantagne-Hurtubise, X.-X. Zhang, and M. Franz, *arXiv:1909.01442*.
- [79] X.-X. Zhang and N. Nagaosa, *Phys. Rev. B* **95**, 205143 (2017).
- [80] Avoiding this, one can instead use imaginary vector potentials that decay at the boundary.
- [81] D. C. Brody, *J. Phys. A* **47**, 035305 (2014).